Dynamic Process of Phase Transition from Wurtzite to Zinc Blende Structure in InAs Nanowires

ARTICLE *in* NANO LETTERS · NOVEMBER 2013

Impact Factor: 13.59 · DOI: 10.1021/nl403240r · Source: PubMed

6 AUTHORS, INCLUDING:

He Zheng
Wuhan University
36 PUBLICATIONS **729** CITATIONS
SEE PROFILE

Jian Wang
University of Nebraska at Lincoln
139 PUBLICATIONS **1,459** CITATIONS
SEE PROFILE

Scott X Mao
University of Pittsburgh
204 PUBLICATIONS **5,516** CITATIONS
SEE PROFILE

NANO LETTERS

Letter

pubs.acs.org/NanoLett

Dynamic Process of Phase Transition from Wurtzite to Zinc Blende Structure in InAs Nanowires

He Zheng,[†,‡] Jian Wang,[*,§] Jian Yu Huang,[∥] Jianbo Wang,[*,‡] Ze Zhang,[⊥] and Scott X. Mao[*,†]

[†]Department of Mechanical Engineering and Materials Science, University of Pittsburgh, Pittsburgh, Pennsylvania 15261, United States

[‡]School of Physics and Technology, Center for Electron Microscopy and MOE Key Laboratory of Artificial Micro- and Nano-structures, Wuhan University, Wuhan 430072, China

[§]Materials Science and Technology Division, MST-8, Los Alamos National Laboratory, Los Alamos, New Mexico 87545, United States

[∥]8915 Hampton Avenue NE, Albuquerque, New Mexico 87122, United States

[⊥]Center for Electron Microscopy, Department of Materials Science, Zhejiang University, Hangzhou 310027, China

Supporting Information

ABSTRACT: In situ high-resolution transmission electron microscopy revealed the precipitation of the zinc-blende (ZB) structure InAs at the liquid/solid interface or liquid/solid/amorphous carbon triple point at high temperature. Subsequent to its precipitation, detailed analysis demonstrates unique solid to solid wurtzite (WZ) to ZB phase transition through gliding of sharp steps with Shockley partial dislocations. The most intriguing phenomenon was that each step is 6 {111} atomic layers high and the step migrated without any mechanical stress applied. We believe that this is the first direct *in situ* observation of WZ−ZB transition in semiconductor nanowires. A model was proposed in which three Shockley partial dislocations collectively glide on every two {0001} planes (corresponds to six atomic planes in an unit). The collective glide mechanism does not need any applied shear stress.

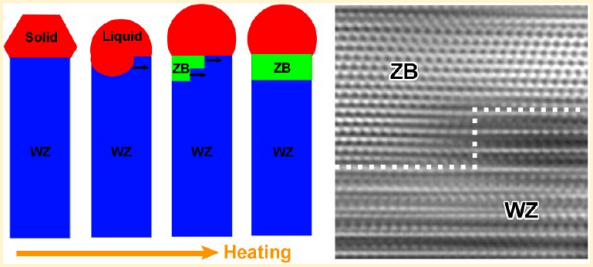

KEYWORDS: *In situ transmission electron microscopy, InAs nanowires, zinc blende, phase transition, dislocation*

As device miniaturization reaches nanometer-length region, one-dimensional III−V compound semiconductor nanomaterials are of great interest because of their novel properties due to the size and quantum-restricted effects and the potential application in nanoscale electronics, optoelectronics, and so forth.[1−3] From the structural point of view, the most surprising feature of the III−V compound nanowires (NWs) is that in sharp contrast to their bulk counterparts, which adopt the cubic zinc blende (ZB) crystal structure, they often exhibit the hexagonal wurtzite (WZ) structure.[4−6] The different stacking sequences of the WZ and ZB structures would yield distinct electronic, photonic and mechanical behaviors of the semiconductor NWs.[7,8] Thus, how to efficiently tailor the structure of III−V nanocompound has stimulated the extensive investigation of the origin of the ZB phase nucleation during the growth of NWs.[9,10] In parallel, it is also highly expected to investigate the structural relationship between the ZB and WZ structures. A natural question to ask is the following: is there any pathway to transform one structure to the other?

Single element face-centered-cubic (fcc) to hexagonal-close-packed (hcp) transition mechanism through partials in alternated two atomic layers was observed in cobalt.[11] Moreover, in a Co-32% Ni single crystal the temperature decreasing could induce a martensitic phase transformation from the fcc to the hcp phase, accompanied by the consecutive glide of partial dislocations with the same Burgers vector, located on every other close packed plane.[12] Regarding the semiconductor NWs, Patriarche et al. recently reported the WZ to ZB structure transition induced by epitaxial burying in GaAs NWs,[13,14] however the related mechanism was unclear due to the lack of real-time observation of the transition process.

Here, through the in situ high-resolution transmission electron microscopy (HRTEM) observation, we found the WZ to ZB phase transition in InAs NWs during the heating process. We believe that this is the first direct visualization of such solid−solid phase transformation in III−V compound semiconductor materials that is induced by the collective gliding of three partial dislocations. A new model is proposed to explain the phase transition without the assistance of external shear stress. Undoubtedly, it provides a new insight into the structural relationship between the WZ and ZB phases in III−V compound materials and further expands its potential application.

Received: August 29, 2013
Revised: November 10, 2013
Published: November 25, 2013

   dx.doi.org/10.1021/nl403240r | *Nano Lett.* 2013, 13, 6023−6027

The Au-catalyzed InAs NWs were grown by metal−organic vapor phase epitaxy (MOVPE) using the vapor−liquid−solid (VLS) technique. The VLS growth mechanism for InAs NWs has been thoroughly investigated.[15] Briefly, a 1 nm thick Au was first deposited onto the (111)B (As-terminated) Si-doped, n-type GaAs wafer by the electron beam evaporation. Afterward, the trimethyl indium (TM In) was introduced to initiate the NW growth at a temperature of 400 °C. After the NW growth, a gold nanoparticle remained on the top of each individual NW. Detailed sample preparation method can be found in ref 16. The as-grown InAs NWs predominantly adopted WZ structure (inset in the Figure 1a, lattice parameter: $a = b = 4.3$ Å, $c = 7.0$ Å) mixed with some stacking faults (pointed out by arrow heads in Figure 1b), which is consistent with the previous experimental observation.[4−6] Besides, each NW was mainly coated with amorphous carbon (Figure 1b), which was unintentionally introduced during the growth period and can act as an excellent heating material.[17] Moreover, carbon exhibits high deformability and strength and thus provides an excellent shielding of the encapsulated materials.[17] The presence of the amorphous carbon coating has also been characterized previously by Pennington et al.[18]

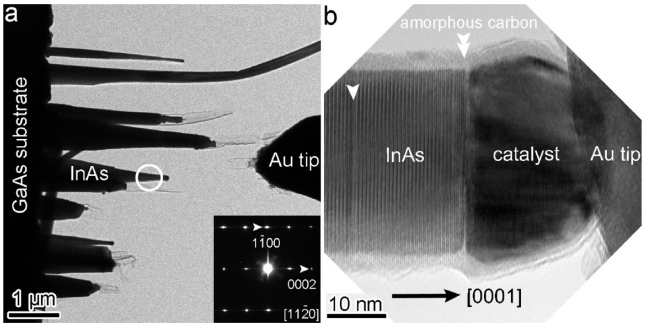

Figure 1. (a) TEM image of the experimental setup, the inset shows the electron diffraction pattern of circled area. (b) High-magnification TEM image showing the contact between the Au tip and InAs NWs with catalyst located at its end. The arrowhead points out the pre-existing stacking fault.

The experiment was performed inside an FEI Tecnai F30 field-emission gun TEM operated at 300 kV. A sample containing many InAs NWs was placed into the electrically grounded Nanofactory TEM-STM platform.[19−21] Because the substrate is electrically conductive, individual NWs can be heated by making electrical contact to the etched gold tip and passing current to ground (Figure 1a). The energy dispersed X-ray spectroscopy (EDS) performed on the seed particle at the tip of the NW indicates that it is mainly consisted of In and Au with the arsenic content below the detection level (Supporting Information Figure S1).

After contacting the gold STM tip with one end of the NW, we started to heat the InAs NW by slowly increasing the voltage and thus the current until the catalyst was melted. Afterward, the applied voltage was kept constant without intentional change. The liquid state of the seed particle can be judged from its curved morphology (Figure 2a) and its molten behavior, as further exemplified by the characteristic halo in the fast Fourier transform image (Supporting Information Figure S2). Subsequently, the liquid particle began to flow and dissolve the InAs NW with WZ structure (Figure 2b). Although the solubility of group V (arsenic in our case) atoms in solid gold is low,[5] our EDS experiments on the liquid droplets revealed the existence of arsenic (Supporting Information Figure S1), in agreement with the previous reports.[22,23] The dashed lines depict the liquid/solid (L/S) interface while arrows point out the moving direction of the interface. Strikingly, when the liquid retracted back along the direction as pointed out by the arrows in Figure 2b, ZB InAs precipitated out at the vicinity of the L/S interface or L/S/amorphous carbon triple point (Figure 2c). The ZB phase has a lattice constant of $a = 6.1$ Å (close to the corresponding value of the bulk ZB InAs: $a = 6.04$ Å[24]). The entire precipitation process can be directly visualized in Supporting Information Movie M1. The crystallographic relationship between the two phases matches well with the expected one between ZB and WZ structure: $(111)_{ZB}//(0001)_{WZ}$, $[1\bar{1}0]_{ZB}//[11\bar{2}0]_{WZ}$ (Figure 2d). Additionally, the growth direction is along $[111]_{ZB}$ while the major growth front corresponds to $(111)_{ZB}$ plane as indicated by the sharp WZ−ZB interface (Figure 2d). For that the nucleation occurred without any solid−vapor interface, the precipitation of pure ZB phase is expected.[10,25,26] The detailed discussion of the precipitation process and the related mechanism will be presented in a separate paper.

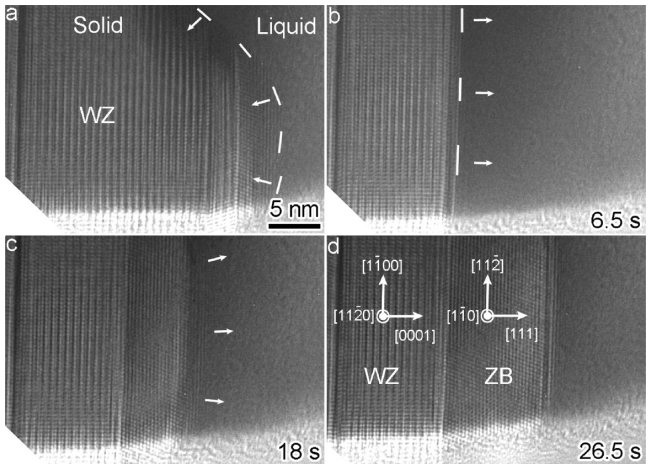

Figure 2. Time-lapsed TEM images showing the dynamic process of the ZB phase precipitation (Supporting Information Movie M1). (a) Initial structure, (b) the liquid particle dissolves one proportion of the InAs NW with original WZ structure, (c) after the liquid retracted back, the ZB-structure InAs partially precipitated out at the vicinity of the L/S interface, and (d) the ZB-structure InAs fully precipitated out at the vicinity of the L/S interface. The dashed lines depict the L/S interface. The arrows point out the moving direction of L/S interface.

More interestingly, once the ZB phase precipitated out, it would propagate along the direction perpendicular to the NW axial direction, thus introducing the WZ to ZB phase transition. Figure 3 shows the full process of the ZB phase propagation assisted by the collective motion of partial dislocations. As a consequence of the liquid swiping through the NW from upper left to lower right (represented by the arrow in Figure 3a), the ZB InAs structure appeared. It is interesting to note that a step was formed along the WZ−ZB interface (pointed out by arrowhead in Figure 3b), which migrated toward the WZ structure and finally disappeared (corresponding to complete phase transformation). It is noted that both phases exhibit crystal structures, that is, both in solid states, implying that this is a solid−solid phase transition (see also Supporting Information Movie M2).

dx.doi.org/10.1021/nl403240r | Nano Lett. 2013, 13, 6023−6027

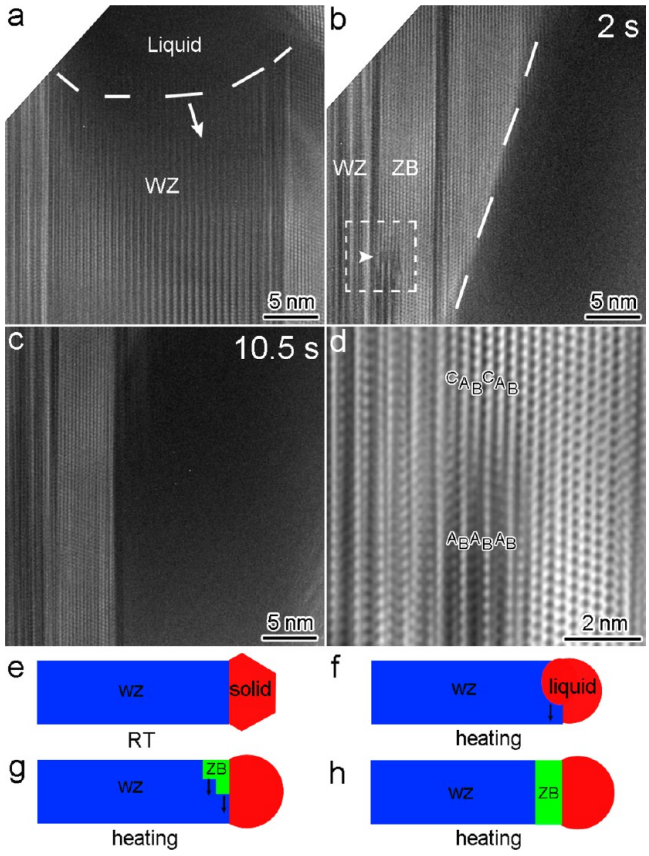

Figure 3. (a–c) Sequential HRTEM images indicating the collective motion of partial dislocations as pointed by the arrowhead in (b), resulting in the phase transition. The dashed lines depict the S–L interface while arrows point out the moving direction of S–L interface. (d) Fourier-filtered image of the white-boxed area in (b). (e–h) Schematic illustration of the precipitation of ZB phase and the subsequent phase transition.

Figure 3e–h shows the schematic presentation of the whole process as described above: first, at room temperature, the catalyst stays in the solid state with faceted surfaces (Figure 3e); second, due to the high temperature the solid catalyst seed (Figure 3e) turns into liquid state (Figure 3f); third, the InAs begins to dissolve into the liquid catalyst while the liquid starts to flow (Figure 3f); finally, the liquid catalyst recedes, then the ZB phase appears (Figure 3g) and propagates along the direction perpendicular to the NW axial direction (Figure 3h). The intriguing phenomena noted here are (1) the step is six {111} atomic layers high, as revealed in HRTEM image; (2) the step is sharp (Figure 3d); and (3) the step migrates without mechanical loading. It is worthy noting that these are frequently observed during the WZ–ZB phase transition.

Here we propose a mechanism in which three Shockley partial dislocations collectively glide on every two {0001} planes (corresponds to six atomic planes in an unit) and have a net zero Burgers vector. Figure 4a shows the {0001} plane stacking in a WZ structure. We symbolized the atomic planes with *A* representing the {0001} atomic plane comprising of In atoms and *a* composing of As atoms. The *A* plane is separated from the *a* plane because As and In atoms are not coplanar. Following the plane stacking in the hcp structure, the {0001} plane stacking in the WZ structure can be denoted as ...*AaBbAaBbAaBb*.... Figure 4b shows the {111} plane stacking in the ZB structure. Similarly, we symbolized the atomic planes with *A* representing the {111} atomic plane comprised of In atoms and *a* composed of As atoms. For comparison, we correspondingly label the {111} plane in the ZB structure as $A(a)$. Following the {111} plane stacking in the fcc structure, the {111} plane stacking in the ZB structure can be denoted as ...$C(c)A(a)B(b)C(c)A(a)B(b)$.... Figure 4c schematically illustrates the phase transition mechanism. Corresponding to conventional understanding, an hcp structure can be transformed into an fcc structure through the glide of Shockley partial dislocation on every two {0001} planes.[27] When shear stress parallel to the {0001} plane is applied, these Shockley partial dislocations likely have same character (gliding along the same direction)[28] or have same edge components with opposite screw components (gliding along the same direction and eliminating the screw strain field).[29] However, both mechanisms do not favor the sharp front of the phase boundary because these dislocations will repulse each other. Corresponding to the experiment condition, there is obviously no shear stress associated with the heating. In addition, the phase boundary is sharp, implying that these dislocations should attract each other. Thus, there is only one possible array of dislocations, as recently verified in fcc $\sum 3\{112\}$ incoherent twin boundary,[28,30,31] in which three Shockley partial dislocations with Burgers vectors b_1, b_2 and b_3 adopt a repeatable order, ...b_2:b_1:b_3..., forming a unit. The Burgers vector of b_1, b_2, and b_3 equals to $1/6[11\bar{2}]$, $1/6[\bar{2}11]$, and $1/6[1\bar{2}1]$, respectively, whereas b_1 corresponds to a pure edge partial dislocation while b_2 and b_3 represent the mixed partial dislocations with opposite sign of screw components. It should be mentioned that the three Shockley partial dislocations in a unit have a net zero Burgers vector. The attractive interaction from the opposite screw components between b_2 and b_3 inhibits them from breaking apart. b_1 is attracted by b_2 and b_3 due to the interaction force resulted from the opposite edge components. Thus, the phase boundary has a minimum thickness of six atomic layers and is compact and sharp. Once the six-layer phase boundary forms, the three Shockley partial dislocations can collectively glide as one unit. The driving force is ascribed to the decrease in bulk cohesive energy because ZB structure has lower bulk cohesive energy than WZ structure.[9] It should be pointed out that the collective glide mechanism is likely when shear stress is not applied, because the energy decreases about 135 meV/nm, corresponding to that a six-layer step when 1 nm thick moves 1 nm.[32] Associated with the glide of Shockley partial dislocations, As and In atoms have to experience shuffles normal to {0001} plane, for example, *Aa* becomes $A(a)$.

Besides, phase transformation takes place from top regions and propagates downward into NW. The key reason is ascribed to the easy of nucleation of the ZB phase at the top surface. The second is related to the release of the phase transformation strain resulting from the change of crystal structure. Theoretically, it is noted that the interplanar distance is 3.516 Å for the {111} plane in ZB structure and 3.520 Å for the {0001} plane in WZ structure, respectively. In association with phase transition, a compressive strain of −0.11% is induced along the [0001] direction. In addition, the {0001} plane and {111} plane have different areal density, leading to in-plane expansion with a displacement gradient of 0.14%. To release the phase transformation strain, the region near free surfaces without constraints is energetically favorable than inside the NWs or other regions far from top surface.

dx.doi.org/10.1021/nl403240r | *Nano Lett.* 2013, 13, 6023–6027

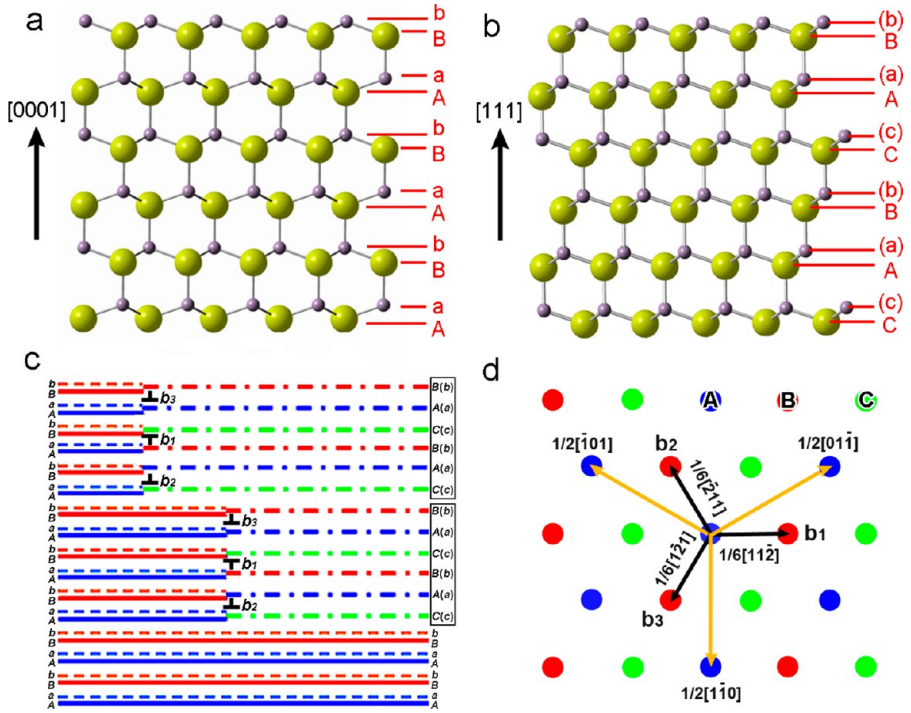

Figure 4. Transition mechanism. Atomic structures, showing (a) {0001} plane stacking in WZ structure with stacking order symbolized as ...*AaBbAaBbAaBb*.... (b) {111} plane stacking in ZB structure, with stacking order symbolized as ...*C*(*c*)*A*(*a*)*B*(*b*)*C*(*c*)*A*(*a*)*B*(*b*).... (c) Schematic illustration of the phase transition mechanism, showing two steps comprising of two sets of dislocations with an order of b_2:b_1:b_3:b_2:b_1:b_3. (d) Three Burgers vectors with the reference of an fcc {111} plane.

For comparison, we have also carried out the heating experiment in InAs NW without the seed particle on its end. Under this circumstance, the InAs NW sublimed at high temperature and no precipitation occurred (see also Supporting Information Movie M3), indicating that the phase transition cannot be solely induced by the high temperature.

In summary, the process of WZ to ZB transition in semiconductor InAs NWs has been found through in situ HRTEM observation. Different from conventional hcp to fcc transition, the observed WZ to ZB transition was through a glide of a step (six atomic layers) in phase boundary. Once the six-layer phase boundary forms, the three Shockley partial dislocations can collectively glide as a unit, where three Shockley partial dislocations forming a unit with a net zero Burgers vector with no shear stress requirement. The driving force for the phase transition is ascribed to the decrease in bulk cohesive energy because ZB structure has lower bulk cohesive energy than WZ structure. Understanding of the WZ to ZB transition mechanism will be important to manipulate the phase transition in the III−V compound NWs to achieve unique electronic and photonic property.

■ ASSOCIATED CONTENT

Supporting Information

Detailed analysis of catalyst composition and the dynamic phase transition movies. This material is available free of charge via the Internet at http://pubs.acs.org.

■ AUTHOR INFORMATION

Corresponding Authors

*E-mail: (S.X.M.) smao@engr.pitt.edu.
*E-mail: (J.W.) wangj6@lanl.gov
*E-mail: (J.W.) wang@whu.edu.cn

Author Contributions

The manuscript was written through contributions of all authors. All authors have given approval to the final version of the manuscript.

Notes

The authors declare no competing financial interest.

■ ACKNOWLEDGMENTS

S.M. would like to acknowledge NSF CMMI 08 010934 through University of Pittsburgh and Sandia National Lab support. J.W. acknowledges the support provided by the U.S. Department of Energy, Office of Basic Energy Sciences. This work was performed, in part, at the Center for Integrated Nanotechnologies, a U.S. Department of Energy, Office of Basic Energy Sciences user facility. Sandia National Laboratories is a multiprogram laboratory operated by Sandia Corporation, a Lockheed-Martin Company, for the U.S. Department of Energy under Contract No. DE-AC04-94AL85000. This research was supported in part by an appointment to the Sandia National Laboratories Truman Fellowship in National Security Science and Engineering sponsored by Sandia Corporation. J.-B.W. would like to thank the financial support from 973 Program (2011CB933300), National Natural Science Foundation of China (51071110, 40972044, 51271134, J1210061), China MOE NCET Program (NCET-07-0640), MOE Doctoral Fund (20090141110059), and the Fundamental Research Funds for the Central Universities. The authors thank Jeffrey G. Cederberg from Sandia National Laboratories for providing the samples and Jesper Wallentin from Lund University and Yang He from University of Pittsburgh for helpful discussion. H.Z. thanks the China Postdoctoral Science Foundation

(2013M540602) and the Chinese Scholarship Council for financial support.

REFERENCES

(1) Duan, X.; Huang, Y.; Cui, Y.; Wang, J.; Lieber, C. M. *Nature* **2001**, *409* (6816), 66−69.
(2) Wang, J.; Gudiksen, M. S.; Duan, X.; Cui, Y.; Lieber, C. M. *Science* **2001**, *293* (5534), 1455−1457.
(3) Gudiksen, M. S.; Lauhon, L. J.; Wang, J.; Smith, D. C.; Lieber, C. M. *Nature* **2002**, *415* (6872), 617−620.
(4) Koguchi, M.; Kakibayashi, H.; Yazawa, M.; Hiruma, K.; Katsuyama, T. *Jpn. J. Appl. Phys.* **1992**, *31* (1), 2061−2065.
(5) Persson, A. I.; Larsson, M. W.; Stenström, S.; Ohlsson, B. J.; Samuelson, L.; Wallenberg, L. R. *Nat. Mater.* **2004**, *3* (10), 677−681.
(6) Larsson, M. W.; Wagner, J. B.; Wallin, M.; Håkansson, P.; Fröberg, L. E.; Samuelson, L.; Wallenberg, L. R. *Nanotechnology* **2007**, *18* (1), 015504.
(7) Chen, B.; Gao, Q.; Wang, Y.; Liao, X.; Mai, Y.-W.; Tan, H. H.; Zou, J.; Ringer, S. P.; Jagadish, C. *Nano Lett.* **2013**, *13* (7), 3169−3172.
(8) Chen, B.; Wang, J.; Gao, Q.; Chen, Y.; Liao, X.; Lu, C.; Tan, H. H.; Mai, Y.-W.; Zou, J.; Ringer, S. P.; Gao, H.; Jagadish, C. *Nano Lett.* **2013**, *13* (9), 4369−4373.
(9) Akiyama, T.; Sano, K.; Nakamura, K.; Ito, T. *Jpn. J. Appl. Phys.* **2006**, *45* (No. 9), L275−L278.
(10) Glas, F.; Harmand, J.-C.; Patriarche, G. *Phys. Rev. Lett.* **2007**, *99* (14), 146101.
(11) Houska, C. R.; Averbach, B. L.; Cohen, M. *Acta Metall.* **1960**, *8* (2), 81−87.
(12) Waitz, T.; Karnthaler, H. P. *Acta Mater.* **1997**, *45* (2), 837−847.
(13) Patriarche, G.; Glas, F.; Tchernycheva, M.; Sartel, C.; Largeau, L.; Harmand, J.-C.; Cirlin, G. E. *Nano Lett.* **2008**, *8* (6), 1638−1643.
(14) Glas, F.; Patriarche, G.; Harmand, J. C. *J. Phys.: Conf. Ser.* **2010**, *209*, 012002.
(15) Dayeh, S. A.; Yu, E. T.; Wang, D. *Nano Lett.* **2007**, *7* (8), 2486−2490.
(16) Seletskiy, D. V.; Hasselbeck, M. P.; Cederberg, J. G.; Katzenmeyer, A.; Toimil-Molares, M. E.; Léonard, F.; Talin, A. A.; Sheik-Bahae, M. *Phys. Rev. B* **2011**, *84* (11), 115421.
(17) Costa, P. M. F. J.; Gautam, U. K.; Bando, Y.; Golberg, D. *Nat. Commun.* **2011**, *2*, 421.
(18) Pennington, R. S.; Jinschek, J. R.; Wagner, J. B.; Boothroyd, C. B.; Dunin-Borkowski, R. E. *J. Phys.: Conf. Ser.* **2010**, *209*, 012013.
(19) Zheng, H.; Cao, A.; Weinberger, C. R.; Huang, J. Y.; Du, K.; Wang, J.; Ma, Y.; Xia, Y.; Mao, S. X. *Nat. Commun.* **2010**, *1* (9), 144.
(20) Zheng, H.; Wang, J.; Huang, J.; Cao, A.; Mao, S. *Phys. Rev. Lett.* **2012**, *109* (22), 225501.
(21) Zheng, H.; Liu, Y.; Mao, S. X.; Wang, J.; Huang, J. Y. *Sci. Rep.* **2012**, *2* (542), 1−4.
(22) Tizei, L. H. G.; Chiaramonte, T.; Ugarte, D.; Cotta, M. A. *Nanotechnology* **2009**, *20* (27), 275604.
(23) Sun, X. *Appl. Phys. Lett.* **2006**, *89* (23), 233121.
(24) Woolley, J. C.; Smith, B. A. *Proc. Phys. Soc.* **1958**, *72* (5), 867.
(25) Dubrovskii, V. G.; Cirlin, G. E.; Sibirev, N. V.; Jabeen, F.; Harmand, J. C.; Werner, P. *Nano Lett.* **2011**, *11* (3), 1247−1253.
(26) Krogstrup, P.; Curiotto, S.; Johnson, E.; Aagesen, M.; Nygard, J.; Chatain, D. *Phys. Rev. Lett.* **2011**, *106* (12), 125505.
(27) Hirth, J. P.; Lothe, J. *Theory of Dislocations*, 2nd ed.; John Wiley and Sons: New York, 1992.
(28) Wang, J.; Anderoglu, O.; Hirth, J. P.; Misra, A.; Zhang, X. *Appl. Phys. Lett.* **2009**, *95* (2), 021908.
(29) Wang, J.; Beyerlein, I. J.; Hirth, J. P.; Tomé, C. N. *Acta Mater.* **2011**, *59* (10), 3990−4001.
(30) Wang, J.; Li, N.; Anderoglu, O.; Zhang, X.; Misra, A.; Huang, J. Y.; Hirth, J. P. *Acta Mater.* **2010**, *58* (6), 2262−2270.
(31) Liu, L.; Wang, J.; Gong, S. K.; Mao, S. X. *Phys. Rev. Lett.* **2011**, *106* (17), 175504.
(32) Zanolli, Z.; Fuchs, F.; Furthmüller, J.; von Barth, U.; Bechstedt, F. *Phys. Rev. B* **2007**, *75* (24), 245121.